DOE/MC/29061-96/C0657

CONF-9510109--27

Rayleigh/Raman/LIF Measurements in a Turbulent Lean Premixed Combustor

Author:

S. P. Nandula
R. W. Pitz
R. S. Barlow
G. J. Fiechtner

Contractor:

South Carolina Energy Research and Development Center
Clemson University
Clemson, SC 29634

Contract Number:

DE-FC21-92MC29061

Conference Title:

Advanced Turbine Systems Annual Program Review

Conference Location:

Morgantown, West Virginia

Conference Dates:

October 17-19, 1995

Conference Sponsor:

U.S. Department of Energy, Office of Power Systems Technology, Morgantown Energy Technology Center

Contracting Officer Representative (COR):

Norman Holcombe

Disclaimer

P2 Rayleigh/Raman/LIF Measurements in a Turbulent Lean Premixed Combustor

S. P. Nandula (nandulsp@ctrvax.vanderbilt.edu; 615-343-6162)
R. W. Pitz (pitzrw@vuse.vanderbilt.edu; 615-322-0209)
Vanderbilt University
Department of Mechanical Engineering
Nashville, TN 37212

R. S. Barlow (barlow@ca.sandia.gov; 510-294-2688)
G. J. Fiechtner (gjfiech@ca.sandia.gov; 510-294-2688)
Sandia National Laboratories
Combustion Research Facility
Livermore, CA 94566

Introduction

Much of the industrial electrical generation capability being added worldwide is gas-turbine engine based and is fueled by natural gas. These gas-turbine engines use lean premixed (LP) combustion to meet the strict NO_x emission standards, while maintaining acceptable levels of CO. In conventional, diffusion flame gas turbine combustors, large amount of NO_x forms in the hot stoichiometric zones via the Zeldovich (thermal) mechanism. Hence, lean premixed combustors are rapidly becoming the norm, since they are specifically designed to avoid these hot stoichiometric zones and the associated thermal NO_x. However, considerable research and development are still required to reduce the NO_x levels (25-40 ppmvd adjusted to 15% O_2 with the current technology), to the projected goal of under 10 ppmvd by the turn of the century. Achieving this objective would require extensive experiments in LP natural gas (or CH_4) flames for understanding the combustion phenomena underlying the formation of the exhaust pollutants. Although LP combustion is an effective way to control NO_x, the downside is that it increases the CO emissions. The formation and destruction of the pollutants (NO_x and CO) are strongly affected by the fluid mechanics, the finite-rate chemistry, and their (turbulence-chemistry) interactions. Hence, a thorough understanding of these interactions is vital for controlling and reducing the pollutant emissions. The present research is contributing to this goal by providing a detailed nonintrusive laser based data set with good spatial and temporal resolutions of the pollutants (NO and CO) along with the major species, temperature, and OH. The measurements reported in this work, along with the existing velocity data (Pan et al., 1991a) on a turbulent LP combustor burning CH_4, would provide insight into the turbulence-chemistry interactions and their effect on pollutant formation.

The literature on nonintrusive measurements of NO_x and CO is very limited, primarily due to the difficulty in measuring small concentrations (~ ppm) of CO and NO. Previous experimental studies of NO_x and CO formation have been based almost entirely on gas-sampling probe techniques (e.g., Drake

Research sponsored by the U.S. Department of Energy's Morgantown Energy Technology Center, under contract DE-FC21-92MC29061 with Clemson University Research Foundation, Box 345702, 300 Bracket Hall, Clemson, SC 29634-5702; telefax: 803-656-1429.

et al., 1987; Driscoll et al., 1992; Vranos et al., 1992). However, the instantaneous relationships between the pollutants and the other scalars which are crucial for evaluating the turbulence-chemistry interactions are lost, since the gas sampling probes provide only averaged measurements. Hence, the data from probes has limited applicability for evaluation and refinement of emissions models of emissions (e.g., characteristic time models, turbulence-chemistry models, and chemical reactor models).

Non-intrusive diagnostics based on Raman scattering has been used successfully by previous researchers (Dibble et al., 1987, 1990; Mansour et al., 1988, 1990, 1991; Masri et al., 1987a, b, c; Stårner et al., 1990) to obtain scalar (species and temperature) measurements in CH_4 flames. These measurements in CH_4 flames have provided a database for evaluation of combustion models and prediction of the turbulence-chemistry interactions (Pope, 1990; Mansour et al., 1989). However, there are no simultaneous laser based multiscalar measurements that include the exhaust pollutants (NO and CO). The clear need for such measurements in methane flames, which would point the way to the effects of turbulence-chemistry interactions in NO and CO formation and guide the development of emissions models and perhaps, reduced chemistry schemes, has prompted this research.

Objectives

The objectives of the research were (i) to obtain simultaneous and instantaneous quantitative nonintrusive laser based measurements with good spatial and temporal resolutions; (ii) to provide insights into the role of the turbulence-chemistry interactions on pollutant (NO and CO) formation in turbulent LP methane-air flames; and (iii) to provide a data base for evaluation and refinement of existing engineering models of emissions for gas-fired, lean premixed combustion turbines. The optical measurements include major species concentrations, temperature, and OH along with the pollutants NO and CO. The nonintrusive diagnostics program is a collaborative effort of Vanderbilt University, Sandia National Laboratories, and Wright Air Force laboratories.

In this paper, we present results of major species (CH_4, O_2, N_2, H_2O, CO_2), temperature, OH, and the pollutants (NO and CO) from a lean premixed bluff body stabilized turbulent combustor burning methane. Extensive measurements ranging from 0.1 diameters to 6 diameters downstream of the bluff body were performed to map the flow field of the combustor. The combustor and the flame parameters were chosen to match the conditions for which Pan and co-workers have reported velocity and temperature measurements using Laser Doppler Anemometry (LDA) and Coherent Anti-Stokes Raman Spectroscopy (CARS) respectively (Pan et al., 1991 a, b, 1992 a, b). These multiscalar measurements, along with the reported velocity measurements will provide insight into the NO_x and CO formation in the combustor.

Approach

The strategy for the Rayleigh/Raman/Laser Induced Fluorescence (LIF) measurements was as follows: spontaneous Raman scattering was used to obtain the quantitative single-pulse major species concentrations and the pollutant CO. In the present experiment (LP CH_4-air environment), the major species were the fuel (CH_4), the oxidizer (O_2 & N_2), and the products (H_2O & CO_2). Temperature was determined from the strong Rayleigh scattering signal which was monitored simultaneously. The Rayleigh signal was converted to temperature by a species weighted scattering cross-section (from the Raman measurements). The Rayleigh scattering cross-sections were calculated from the index of refraction data of Gardiner (Gardiner et al., 1981). The minor

species, OH and NO, were measured by separate lasers using linear (or near-linear) laser induced fluorescence. The LIF signals from the minor species (NO and OH) were then corrected on a single-shot basis for quenching (which is species dependent) and population fraction (which is temperature dependent), to obtain their quantitative values. Temperature was also obtained for each laser shot from the measurements of species concentrations by invoking the perfect gas law.

Diagnostic System

A schematic of the experimental system is shown in Fig. 1. The lean premixed combustor was mounted at the exit of a vertical wind tunnel contraction which could be translated along the three axes. The beam from a Nd:YAG laser (532 nm, ~750 mJ/pulse, 5 Hz) was used for Raman (major species and CO) and Rayleigh (temperature) measurements. This laser has a pulse length of 5 ns which is stretched to 200 ns to avoid laser induced breakdown at the focal volume. The LIF measurements of minor species (NO and OH) were accomplished with two separate Nd:YAG-pumped dye laser systems. A fourth Nd:YAG laser system shown in the figure for measurements of CO by LIF (higher accuracy) will be incorporated in the next set of measurements (scheduled for May, 1996). The three laser beams were combined into a common axis, using two dichroic mirrors, and focused into

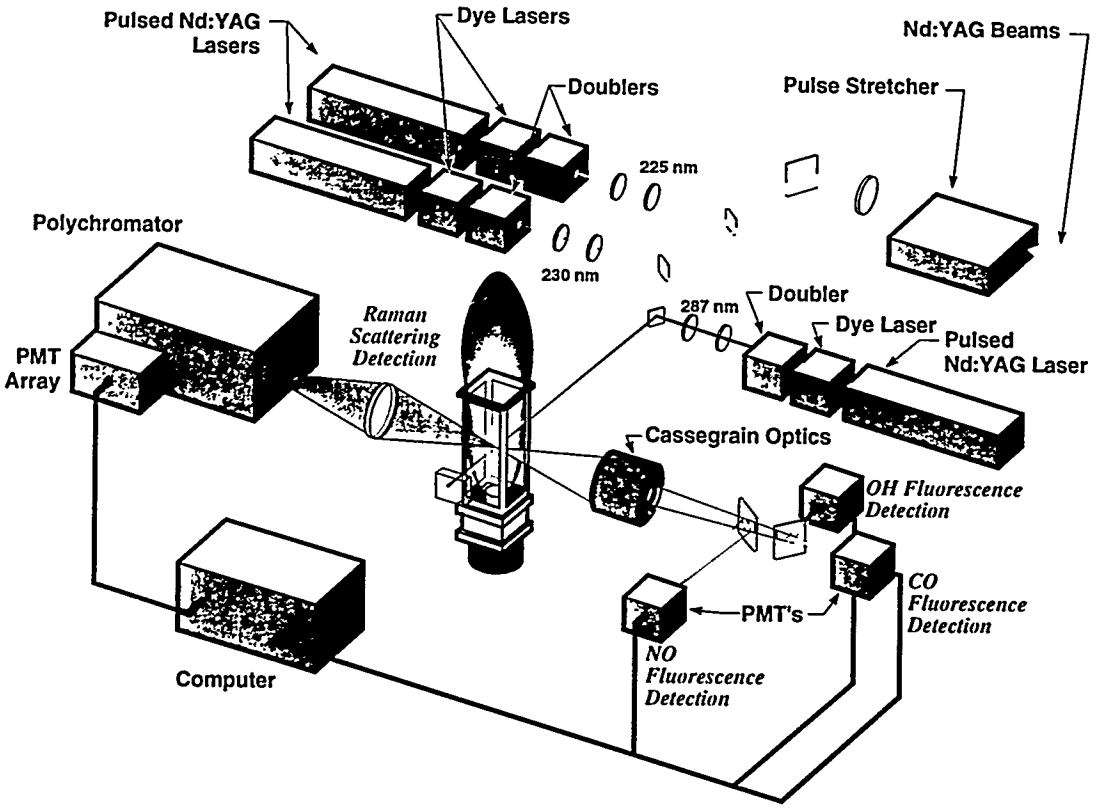

Fig. 1. Schematic of the Rayleigh/Raman/LIF diagnostic system.

the test section. The 532 nm beam was retro-reflected into the measurement volume using a prism to effectively double the Rayleigh and Raman signals. The spatial resolution of the measurements was ~ 800 μm in each direction, and the delays between each of the three pulses were ~1 μs. The laser firing sequence was as follows: NO laser, followed by the OH laser and finally the 532 nm laser for Rayleigh/Raman measurements.

The scattered Raman and Rayleigh signals were collected using a six-element achromat and collimated using a conventional camera lens. The collimated light was relayed to photomultiplier tubes (PMT's) aligned at the exit plane of a 0.75-m spectrometer. Fluorescence signals from OH and NO were collected using Cassegrain optics located on the other side of the test section as shown in Fig. 1. A dichroic mirror separated and relayed the NO and OH fluorescence signals to separate detectors.

For OH excitation-detection, the frequency-doubled output for one of the dye lasers was tuned to the $O_{12}(8)$ transition in the $A^2\Sigma^+ - X^2\Pi$ (1, 0) band (λ = 287.9 nm). Colored glass filters were placed in front of the OH detector to capture much of the fluorescence from the dominant (1, 1), (1, 0), and (0, 0) bands, where the (0, 0) fluorescence is preceded by vibrational energy transfer. For NO excitation, the second dye laser was tuned to the $R_1(18)$ transition in the $A^2\Sigma^+ - X^2\Pi$ (0, 0) band. This state is reasonably isolated from the neighboring NO lines, and the ground state is populated over a wide range of temperatures, including room temperature. A solar-blind PMT (Hamamatsu R166) and Schott UG-5 colored glass filters were used for detection of NO signals. This arrangement allowed collection of fluorescence from the system of NO bands at 236, 247, 259, and 271 nm. The NO measurements were performed with a slight degree of saturation, which were accounted and corrected during data processing.

Wavelengths of the laser beams of NO and OH were each monitored indirectly by measuring fluorescence from two small premixed CH_4-air flames. The line widths and shifts of the two dyes lasers were constantly monitored during the course of the measurements and were adjusted as necessary to remain line-centered on the NO and OH transitions. Detailed descriptions of the experimental system have been reported previously (Barlow et al., 1990; Barlow and Carter, 1994).

Signal Calibration

The diagnostic system was calibrated for temperature dependent calibration factors and cross-talk between the Raman channels, to convert the raw signals to absolute species concentrations and temperature. This was accomplished by measuring signals in laminar adiabatic flames over a wide range of equivalence ratios. The O_2, N_2, H_2O, and H_2 Raman signals and the OH LIF signals were calibrated in H_2-air flames over an uncooled multi-element Hencken burner for equivalence ratios ranging from 0.2 (fuel lean) to 1.7 (fuel rich). The heat loss from the burner is negligible at sufficiently high flowrates and the flowfield at this location (~4 cm downstream) is uniform and at adiabatic equilibrium. The radiative heat losses in H_2-air flames for this burner are ~20-40 K. The calibration results are shown in Fig. 2. The lines in the figure show laminar adiabatic equilibrium calculations obtained using STANJAN (Reynolds, 1986). The calibrations show good agreement with the theoretical equilibrium curves. The single-pulse standard deviations of species concentrations, temperature, and mixture fraction are shown as error bars in Fig. 2.

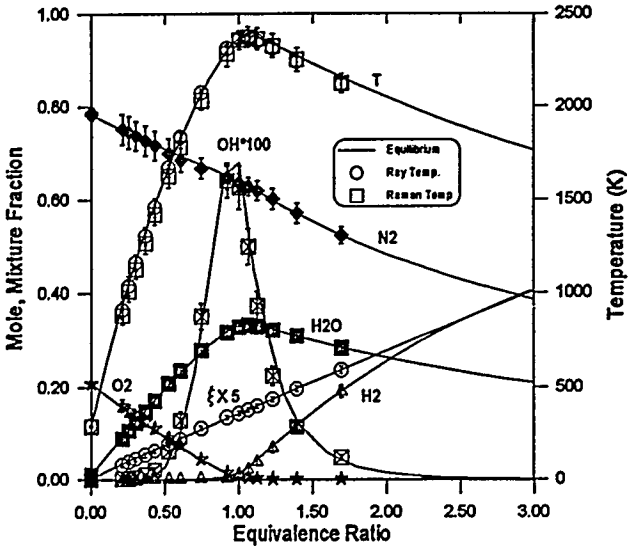

Fig. 2. Calibration results of the major species concentrations (O_2, N_2, H_2O, and H_2), OH, and temperature at various equivalence ratios in a laminar H_2-air flat flame. The lines show calculations for a laminar equilibrium flowfield. The error bars denote the single-shot uncertainty (± one standard deviation) in the measurements.

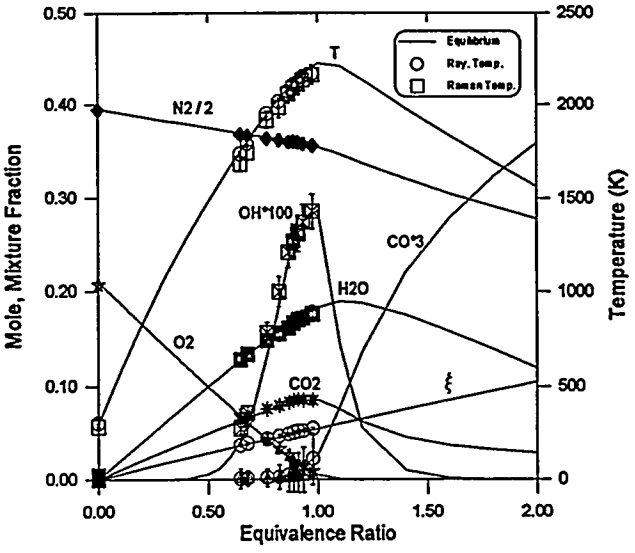

Fig. 3. Calibration results of the major species concentrations (O_2, N_2, H_2O, CO_2, and CO), OH, and temperature at various equivalence ratios in a laminar CH_4-air flat flame. The lines show calculations for a laminar equilibrium flowfield. The error bars denote the single-shot uncertainty (± one standard deviation) in the measurements.

Similar calibrations were performed in CH_4-air flames over the Hencken burner. The Raman signals from O_2, N_2, H_2O, CO_2, CO and the LIF signals from OH were calibrated in this flame. The radiative heat losses in CH_4 flames in the burner are slightly higher (~ 30-50 K) than those of the hydrogen flames due to the presence of CO_2. The calibration results in CH_4 flames are shown in Fig. 3. Thus temperature dependent calibration factors are derived for all the major species that are monitored except CH_4, since CH_4 decomposes readily even at moderate temperatures and no CH_4 is present even in rich CH_4 flames. Therefore, a constant calibration factor which was measured in CH_4 at ambient temperature was used.

The NO system was calibrated using laminar $CH_4/N_2/O_2$ flames over a McKenna burner. Naturally occurring NO concentrations in these flames are very small (~7 ppm) for reliable calibration of the diagnostic system. Hence, these flames are doped with known concentrations of NO (~ 30 ppm) for calibration of the NO LIF system. The flame was so chosen because the destruction of doped NO in these flames is small (Reisel et al., 1993). Detailed descriptions of calibration procedures have been documented in the literature (Barlow and Carter, 1994).

Measurement Uncertainty and Shot Noise

The single-shot uncertainties in the measurements were obtained from standard deviations of the measurements performed in the laminar adiabatic flame of the Hencken burner which was used for system calibration. Typical single-pulse uncertainties of species concentrations, temperature, and mixture fraction (ξ) are shown in Figs. 2 and 3 as error bars (± one standard deviation). The uncertainties are primarily due to the shot noise resulting from the photoelectron emission process of the photocathode. However, these uncertainties also include contributions from the instrument noise and fluctuations in the flame conditions.

In addition to these uncertainties, the LIF measurements (OH and NO) are subject to systematic errors due to the wavelength drift of the dye lasers from the line center. The maximum resulting uncertainties are estimated to be ~5% for OH and 10% for NO. The sensitivity of the NO LIF system is sufficient to obtain useful measurements below 10 ppm.

LP Combustor and Flame Parameters

Fig. 4 shows the combustor which was used for the experiments. Fuel (CH_4) and air are premixed upstream (~3 m) and the cold premixed fuel-air mixture is injected radially at the base of the combustor. Screens and honeycombs are placed in the combustor to make the flow uniform. A stainless steel conical bluff body of base diameter (d = 44.45 mm) and apex angle (θ = 45°) served as the flame stabilizer. The bluff body was mounted coaxially in a 79 mm x 79 mm x 284 mm combustor test section. The blockage ratio with this configuration was 25%. The test section has rounded corners with four

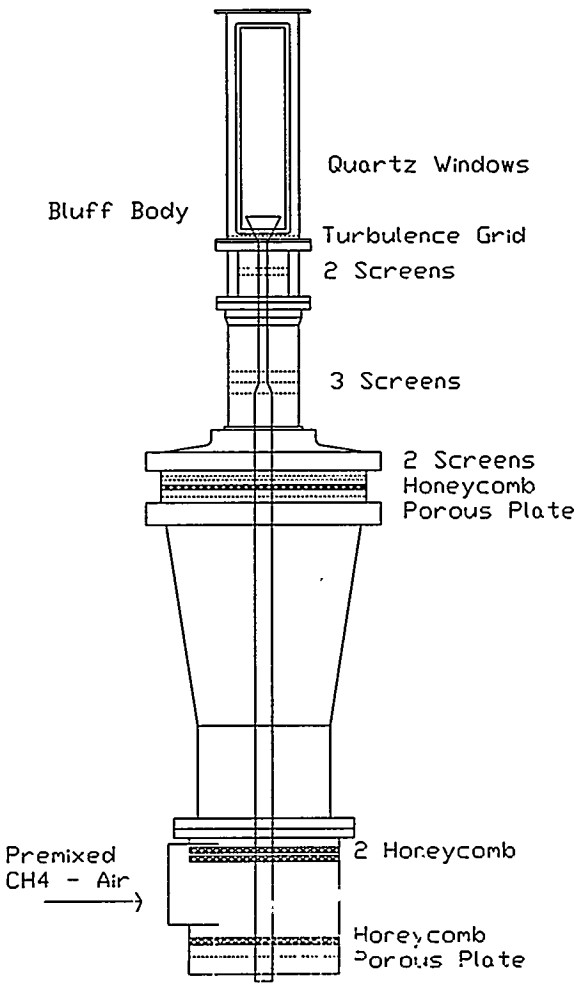

Fig. 4. Schematic of the bluff-body stabilized lean premixed CH_4-air turbulent combustor.

56.4 mm x 254 mm cutouts for mounting windows. Quartz windows were mounted on the signal receiving side of the diagnostic system. However, on the other side (where the laser beams pass through), the quartz windows were replaced by windows made of high temperature resistant (~2000° F) fiberfrax. This was primarily due to the fact that the energy density of the 532 nm YAG laser was higher than the damage threshold of the quartz windows. Small holes of 9.5 mm diameter were drilled through the fiberfrax to

let the three laser (YAG and dye) beams to pass through. Small holes were chosen so that they would not significantly alter the flowfield in the combustor and still let the laser beams to pass through with sufficient clearance. A turbulence grid was placed at the entrance of the section at 58 mm upstream of the bluff body. The reference velocity at the entrance of the test section in this configuration was 15 m/s. The free stream turbulence and the velocity ratio (u_{rms}/S_L) are 24% and 30 respectively. The combustor is mounted on a vertical wind tunnel contraction which could be traversed along three axes.

The flame parameters in the present experiment correspond to an air flow rate of 3962 slpm (standard liters per minute) and fuel (CH_4) flow rate of 244 slpm, resulting in an equivalence ratio (ϕ) of 0.586 and an adiabatic flame temperature (T_{ad}) of 1641 K. The combustor produces a cone-stabilized premixed flame, which is shown in Fig. 5. The flame is stabilized by the bluff body (cone), with a recirculation zone which extends to about a diameter downstream, a shear layer or an annular flame zone, and a post flame zone. Rayleigh/Raman/LIF measurements were performed at various axial and radial locations on the combustor. In addition to the optical measurements, the pollutants (CO and NO_x) in the exhaust plane (x/d = 6.0) were measured with gas sampling probes. Table 1 summarizes the optical and gas sampling probe measurements. For brevity, only measurements at locations shown in bold (see Table 1) are presented in this paper.

Shadowing. Shadowing factors for the Raman, Rayleigh, and LIF signals were measured at each axial location, to account for the change in the solid angle of collection and obstruction of the signal due to the bluff body and/or the test section. Typical shadowing of the signals at 0.1 diameters downstream are

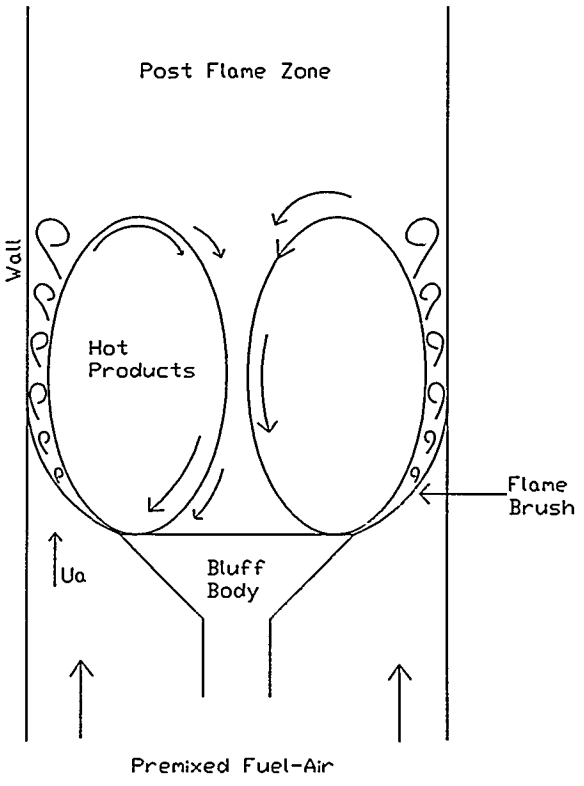

Fig. 5. Turbulent flame structure enveloping the recirculation zone of the bluff body stabilized combustor.

shown in Fig. 6. It is evident from the figure that at radial locations greater than 0.50 diameters, the signals decrease due to test section shadowing. A greater concern with shadowing was the increase in the Rayleigh background at large r/d. The Rayleigh background is almost seven-fold at x/d = 0.55 relative to x/d = 0 (see figure). This Rayleigh background signal is primarily due to the surface scatter from the location where the YAG laser clears the hole in the fiberfrax window. The 532 nm laser beam used for monitoring the Rayleigh signal is focused into the sample volume at a small angle, in order to accommodate retroreflection (see Fig. 1). Therefore, as the burner is traversed radially outward (which corresponds to moving the burner towards/away from the laser beam), the

Table 1. Summary of optical and gas sampling probe measurements.

Measurements	Streamwise location (x/d)	Comments
Optical Diagnostics (Major Species[§], temperature, CO, OH, and NO)	**0.1**, 0.3, **0.6**, 0.8, 1.0, 1.2, 1.5, 2.0, **6.0** (exhaust plane)	Radial profiles at intervals of r/d = 0.05
Gas sampling probes (NO/NO_2 and CO)	**6.0** (exhaust plane)	Radial profiles at intervals of r/d = 0.1

§ Major species denote CO_2, CH_4, H_2, O_2, N_2, and H_2O.

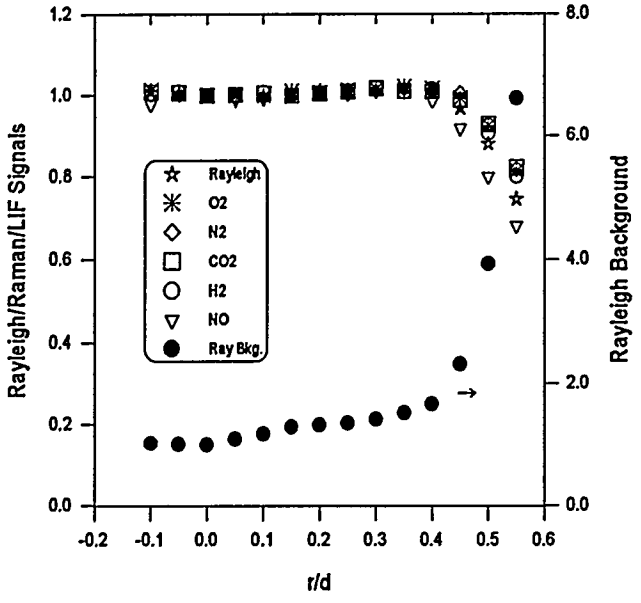

Fig. 6. Typical radial profiles of the Rayleigh/Raman/LIF shadowing factors and the Rayleigh background at x/d = 0.1.

laser beam does not clear the hole as it would at r/d = 0. Moreover, this shadowing of the Raman/LIF signals and the increase in the Rayleigh background were a function of the axial location. Therefore, the shadowing factors were quantified at each location and accounted for during data processing.

Results and Discussion

Radial profiles of the average major species mole fractions, temperature, mixture fraction, CO, OH, and NO at x/d = 0.1 are shown in Fig. 7. The bluff body and the quartz window (denoted as wall) are shown in the figure to facilitate the physical visualization of the combustor. The equilibrium values of the species concentrations, and temperature corresponding to the operating equivalence ratio (0.586) are also shown in the figure. Typically 600-1000 laser shots were registered at each radial location. In the recirculation zone (r/d < 0.5), the mean values of the species and temperature are fairly constant and close to their equilibrium values. The temperature in the recirculation zone (1540 K) is ~6% less than the adiabatic equilibrium temperature (1641 K). The results suggest that the recirculation zone loses about 6% of its heat to the environment, part of it to the bluff body.

Almost half a century back, Longwell proposed that the recirculation zone can be modeled as a "perfectly well stirred reactor" (Longwell et al., 1953). The results suggest that the recirculation zone is almost, but not "perfectly well stirred". More recently,

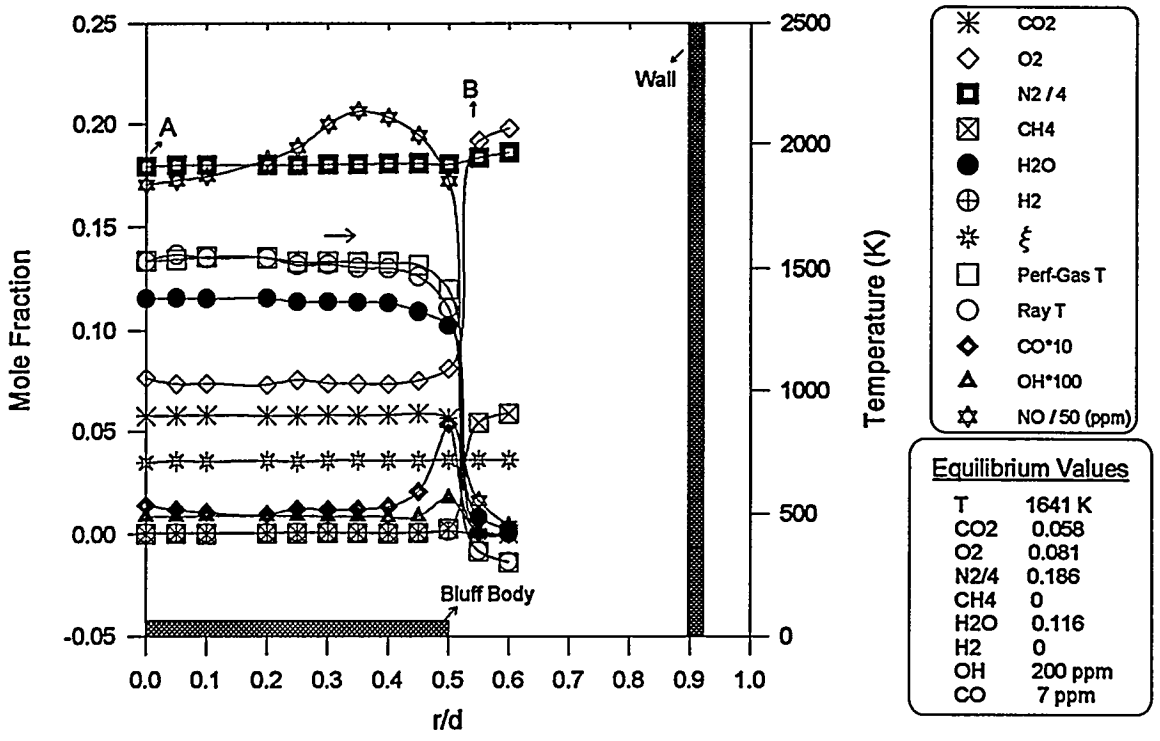

Fig. 7. Radial profiles of the mean species mole fractions, temperature, and mixture fraction at x/d = 0.1.

modellers (Swithenbank et al., 1980; Pratt, 1980) have proposed models of "partially stirred reactors (PSR)" and "imperfect micro-mixing". In these models the recirculation zone is modeled a PSR with a certain fuel-air recycle from the outside. Hitherto, due to the lack of measurements, modellers have assumed and modeled the recirculation zone with recycle ratios ($1 - T/T_{ad}$) of ~10-30%. However measurements from Fig. 7 show that the recycle ratio is 6% (1 - 1540/1641). This indicates that the breakthrough of fuel and air through the shear layer into the recirculation zone is much smaller than what the modellers believed. At r/d > 0.5, the temperature drops steeply from 1600 K to ambient (300 K). This cold reactant region is characterized by the unburnt fuel ($X_{CH4} = 0.05$), air ($X_{N2} = 0.76$, $X_{O2} = 0.19$), and the absence of products (H_2O and CO_2) and intermediate radicals (OH, CO, and NO). In the region between the recirculation zone and the cold premixed fuel/air lies a thin annular flame. The presence of this flame zone can be seen from the hydroxyl (OH) profile which peaks to 200 ppm at r/d = 0.5, which corresponds to the edge of the bluff body. The radial profile of CO also peaks at this point, with the peak CO values of 5000 ppmv. The CO concentrations based on equilibrium concentrations are very small (7 ppmv). This clearly points to the need of well refined engineering models that can accurately predict the pollutants in LP gas turbines. The NO concentrations in this region are relatively small, ~10 ppmv.

The radial profiles of the rms of the species and temperature are shown in Fig. 8. The profiles are fairly constant in the recirculation zone (r/d < 0.5). The rms profiles of fuel (CH_4), oxidizer (O_2, N_2), and temperature peak at r/d = 0.55, the region where the cold premixed fuel-air from regions of r/d > 0.55 exchanges heat and mass to the hot combustion products of the recirculation zone. Note that the rms of Rayleigh temperature is smaller

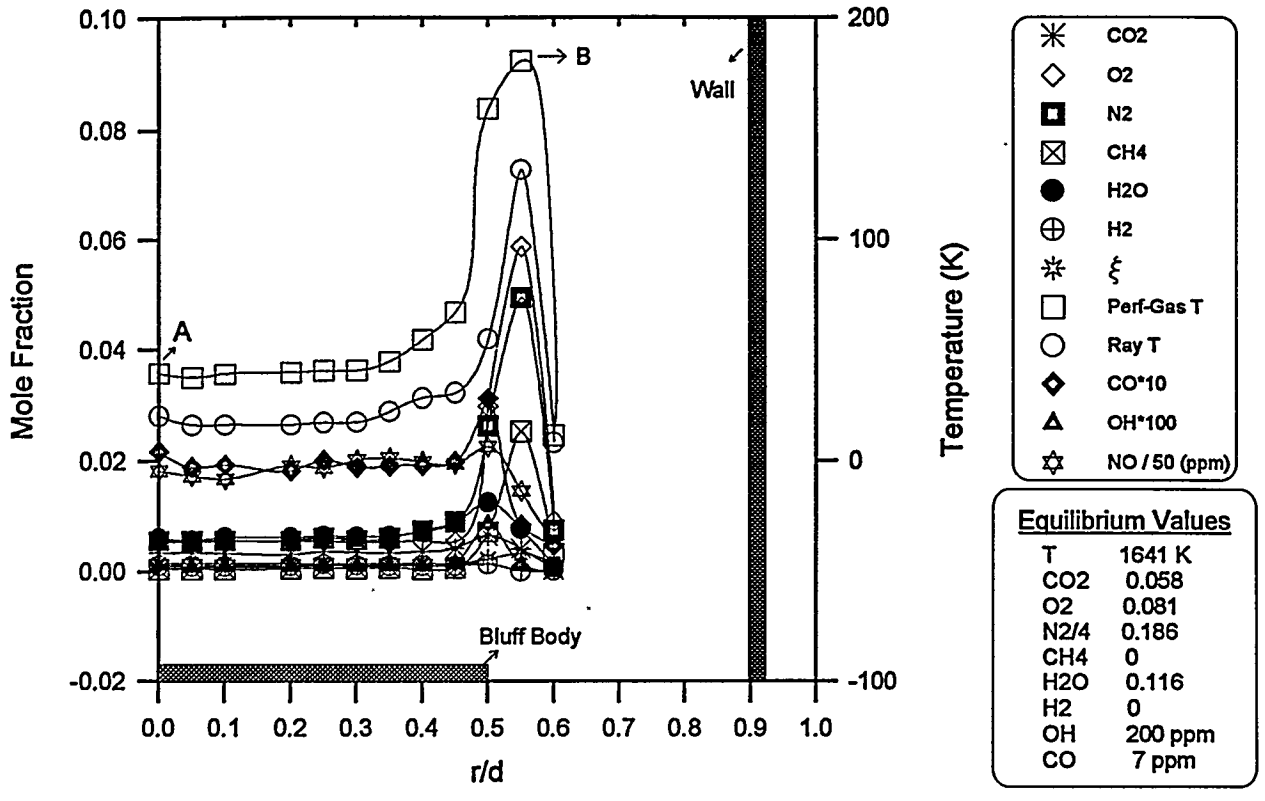

Fig. 8. Radial profiles of the rms species mole fractions, temperature, and mixture fraction at x/d = 0.1.

than that of the Raman perfect gas temperature (temperature calculated from the Raman species concentrations by invoking the perfect gas law). This is primarily due to reduced shot noise in the strong Rayleigh signals as opposed to the Raman signals. The rms profiles of the products (CO_2 and H_2O), the intermediate radical species (OH), and the pollutants (NO and CO) peak slightly inward at x/d = 0.5, the region of the annular flame zone (see OH profile of Fig. 7).

Scatter plots of the measured species mole fractions corresponding to points A and B in Fig. 7 (or 8) are plotted versus temperature in Figs. 9 and 10. Each scatter plot shown is an ensemble of 800 laser shots. Scatter plots such as these provide an overview of the chemistry as each point gives an instantaneous picture of the flame. The horizontal lines in the figures are the adiabatic equilibrium values of the major species (CH_4, O_2, CO_2, and H_2O) and OH corresponding to an equivalence ratio of 0.586. The data in the recirculation zone (Fig. 7) is confined to a narrow temperature band (~250 K). Moreover, the major species mole fractions are very close to their equilibrium values; the oxidizer (O_2) and N_2 (not shown here) are slightly below equilibrium and the products (H_2O and CO_2) are at superequilibrium. All the traits in the data are consistent with the well-stirred reactor concept of the recirculation zone. The CO, OH, and NO concentrations at this location are 740 ppm, 100 ppm, and 5 ppm respectively. In contrast to point A, which is in the recirculation zone, the data at point B (Fig. 10) lies over a broad range of temperature ranging from ambient (300 K) to adiabatic equilibrium temperature (1641 K), due to the turbulent mixing of the cold reactants with hot products. The residence times at this point are small,

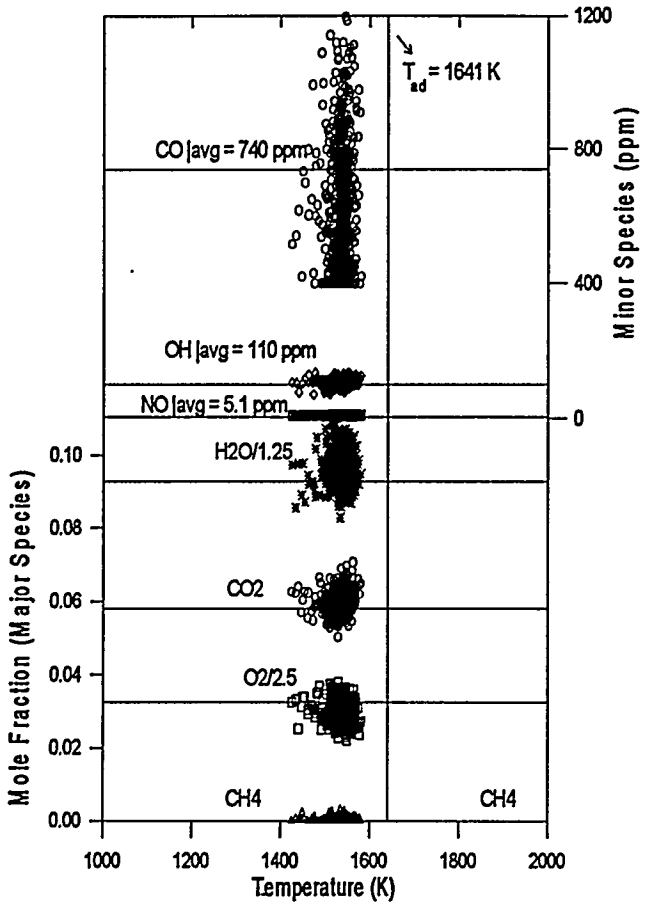

Fig. 9. Scatter plots of measured species mole fractions versus temperature in the combustor at x/d = 0.1 and r/d = 0 (Point A of Figs. 7 and 8). The equilibrium compositions of the major species and OH corresponding to an equivalence ratio of 0.586 are shown.

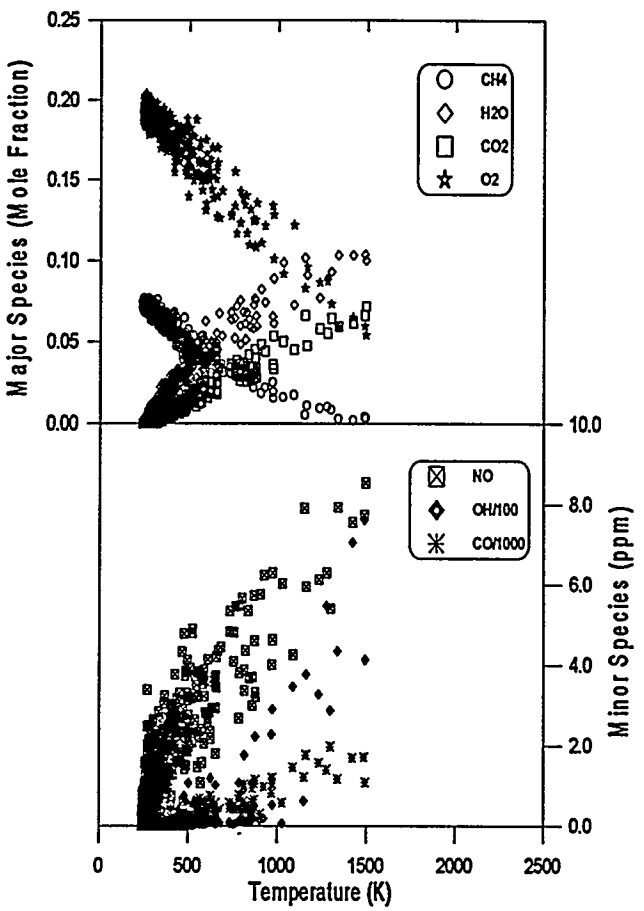

Fig. 10. Scatter plots of measured species mole fractions versus temperature in the combustor at x/d = 0.1 and r/d = 0.55 (Point B of Figs. 7 and 8). The equilibrium compositions of the major species and OH corresponding to an equivalence ratio of 0.586 are shown.

and this can be seen by the high intermediate radical concentrations. Superequilibrium OH values of 800 ppm, up to 4 times the equilibrium values (200 ppm) were recorded. The peak CO concentrations are ~2000 ppm, and the peak NO concentrations are ~10 ppm.

Mean and rms radial profiles of the species concentrations, and temperature at x/d = 0.6 are shown in Figs. 11 and 12. There are no significant differences in the mean and rms measurements of the major species and temperature, when compared to their counterparts at x/d = 0.1 (see Fig. 7). The results are consistent with the heat transfer arguments invoked earlier. However, the maximum NO concentrations at this location are ~8 ppm, slightly smaller from the peak values of 10 ppm at x/d = 0.1. The OH and CO profiles are broader than their corresponding counterparts at x/d = 0.1. This shows evidence of shear layer growth as we move downstream.

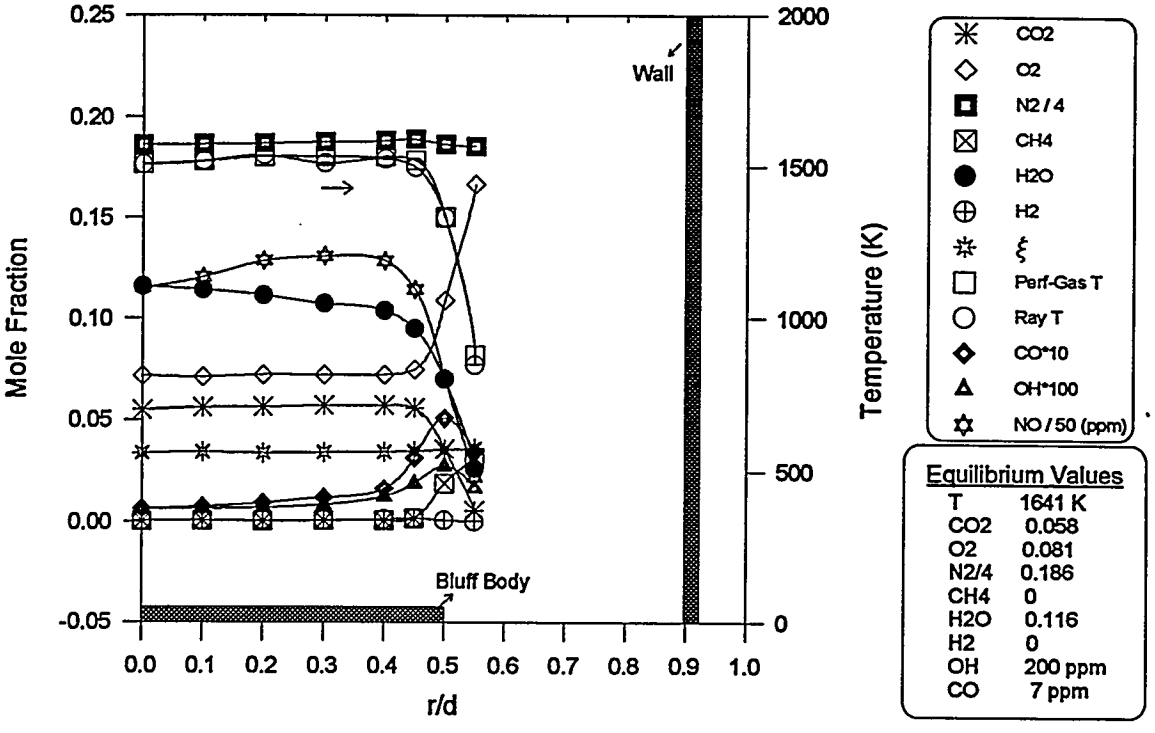

Fig. 11. Radial profiles of the mean species mole fractions, temperature, and mixture fraction at x/d = 0.6.

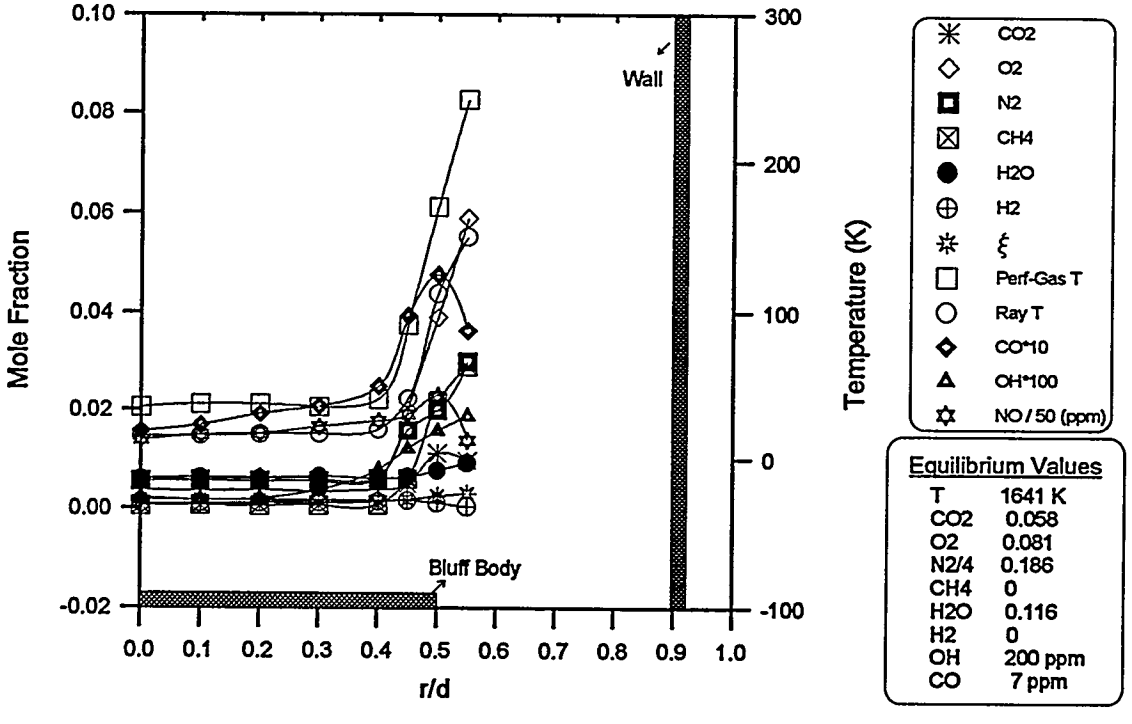

Fig. 12. Radial profiles of the rms species mole fractions, temperature, and mixture fraction at x/d = 0.6.

The shear layer growth is caused by the entertainment process, where isolated pockets of hot products (from the recirculation zone) and cold reactant gases (from the premixed fuel-air stream) are entrained into the shear layer (Pan et al., 1991b).

The mean and rms radial profiles at the exhaust plane of the LP combustor (x/d = 6.0) are shown in Figs. 13 and 14. At this downstream location where there has been sufficient time for the reactants to combine, the major species and temperature are fairly constant across the burner and correspond to adiabatic equilibrium values. The CO concentrations increase as we approach the wall. This increase in the CO concentrations is possibly due to quenching effects from the cold wall. The exhaust plane NO concentrations are about 6 ppm.

Probe Measurements. The exhaust pollutants (NO/NO_x and CO) were also measured with gas sampling probes. The NO/NO_x measurements were performed with a chemiluminescent gas analyzer, and CO was measured with a nondispersive infrared (NDIR) detector. Probe descriptions and calibration procedures have been reported previously in great detail (Mellor, 1994). Optical and gas sampling probe measurements of the exhaust pollutants (NO and CO) at x/d = 6 are shown in Fig. 15. The laser based (LIF) NO measurements agree with the gas sampling probe measurements within 2 ppm. However, the CO concentrations measured with the laser are about 10 times larger than the corresponding probe measurements. The reduced CO concentrations in the probe measurements are due to the oxidation of CO to CO_2 in the warmer sections of the probe via the reaction, CO + OH $\rightarrow$ CO_2 + H. The oxidation of CO to CO_2 in gas sampling probes have been reported in the literature (Kramlich and Malte, 1978; Nguyen et al., 1994). In lean premixed flames where there are considerable CO

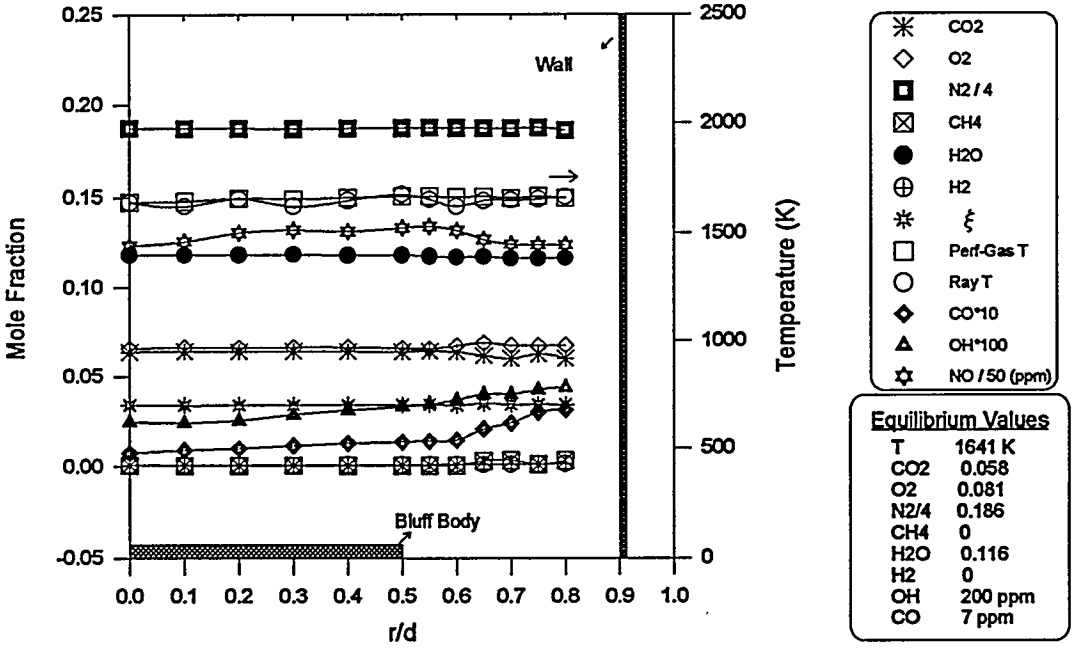

Fig. 13. Radial profiles of the mean species mole fractions, temperature, and mixture fraction at x/d = 6.0.

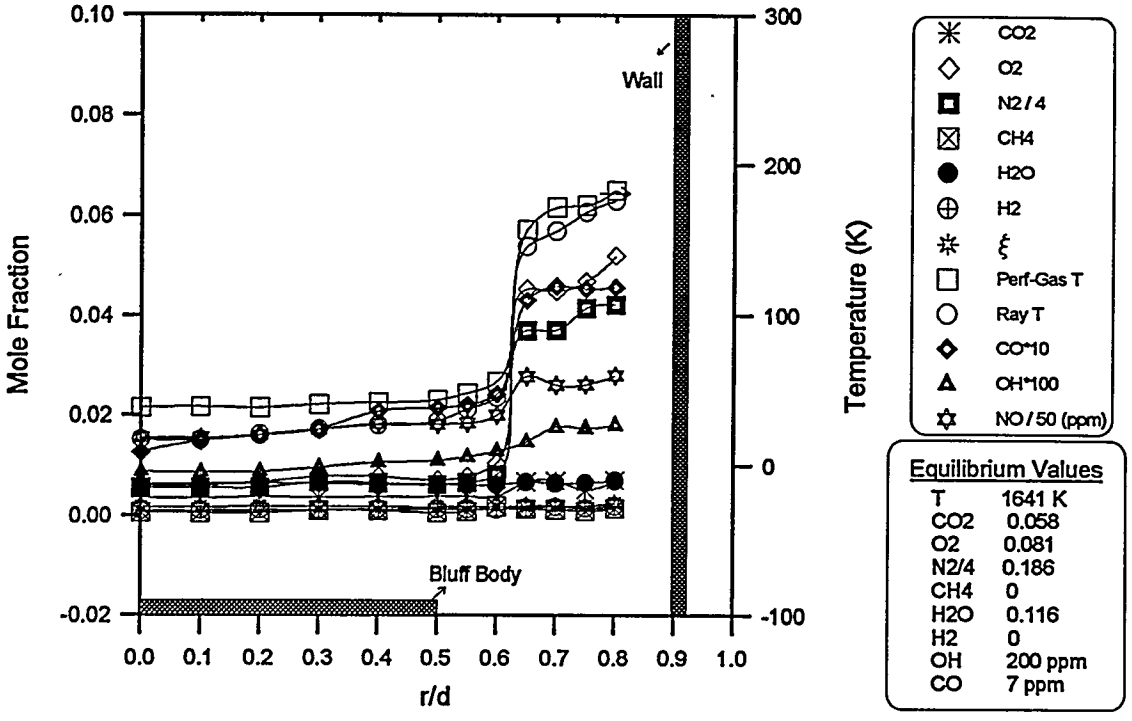

Fig. 14. Radial profiles of the rms species mole fractions, temperature, and mixture fraction at x/d = 6.0.

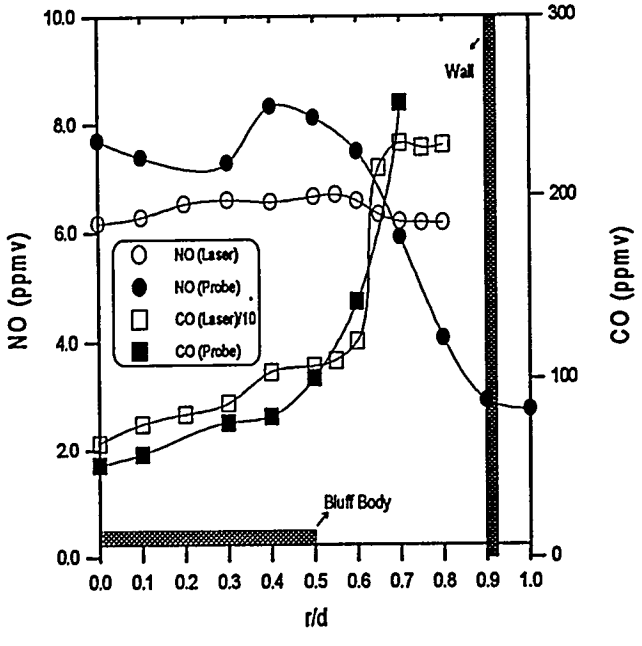

Fig. 15. Laser based and gas sampling probe measurements of exhaust pollutants (NO and CO) at x/d = 6.0.

concentrations, the extraction gas sampling probes can be increasingly inaccurate.

Conclusions

Simultaneous and instantaneous time-resolved point measurements of major species (CO_2, CH_4, H_2, O_2, N_2, and H_2O) concentrations, temperature, and minor species (CO, NO and OH) concentrations were obtained using a combination of spontaneous Raman scattering, Rayleigh scattering, and laser-induced fluorescence in a turbulent lean premixed methane combustor. The fluorescence signals of NO and OH were corrected for Boltzman fraction and collisional quenching rates on a shot-to-shot basis. The detection limit of the NO measurements was ~4 ppm at 1550 K (Number density of 2 x 10^{13} cm^{-3}) in a calibration flame.

The results of species concentrations and temperature in the recirculation zone show that the recirculation is not a perfectly stirred reactor. Measurements indicate that the recirculation resembles a partially stirred reactor. The measured recycle ratio in the recirculation is ~6%. This is quite different from the recycle ratios of 10-30% which the modellers are currently using to model LP gas turbines. This suggests that the breakthrough of the reactants into the recirculation quite small (~6%) as opposed to the nominal value of 25% used in the models. Annual shear layer growth by the edge of the recirculation zone was evident with downstream distance.

Measurements of NO in the exhaust plane (x/d = 6) of the combustor revealed relatively low concentrations of NO (~6 ppm). However, the CO concentrations in the exhaust were high ~1000 ppm. The laser based measurements of CO were about 10 times larger than the gas sampling probe measurements. This suggests that the catalytic reactions in the probe make extraction probe techniques for CO measurement quite inaccurate.

Currently, CO is measured by Raman scattering. However, the CO Raman signals are weak, resulting in poor measurement accuracy. In the next set of measurements, CO will be measured by LIF. Furthermore, the turbulence levels will be varied by varying the free-stream turbulence, and measurements of species, temperature, OH, NO, and CO will be performed. The effects of the variation in the blockage ratio and turbulence intensity on pollutant formation will be investigated.

Acknowledgments

This research was funded by the U.S. Department of Energy Technology Center under Contract No. DE-FC21-92MC29061, for the period of performance beginning September 1, 1993 and ending August 31, 1996. The work at Sandia National Laboratories was supported by the United States Department of Energy, Office of Basic Energy Sciences. The authors wish to acknowledge the METC Contracting Officer's Representative, Dr. Norman Holcombe. We also thank Dr. Mel Roquemore of Air Force Wright Laboratories, for lending the LP combustor.

References

Barlow, R. S., Dibble, R. W., Chen, J. Y., and Lucht, R. P. (1990), *Combustion and Flame* **82**, pp. 235-251.

Barlow, R. S., and Carter, C. D. (1994), *Combustion and Flame* **97**, pp. 261-280.

Dibble, R. W., Masri, A. R., and Bilger, R. W. (1987), *Combustion and Flame* **67**, pp. 189-206.

Dibble, R. W., Stårner, S. H., Masri, A. R., and Barlow, R. S. (1990), *Applied Physics B* **51**, pp. 39-43.

Drake, M. C., Correa, S. M., Pitz, R. W., Shyy, W., and Fenimore, C. P. (1987), *Combustion and Flame* **69**, pp. 347-365.

Driscoll, J. F., Chen, R. H., and Yoon, Y. (1992), *Combustion and Flame* **87**, pp. 37-49.

Gardiner, W. C., Hidaka, Y., and Tanzawa, T. (1981), *Combustion and Flame* **40**, pp. 213-219.

Kramlich, J. C., and Malte, P. C. (1978), *Combustion Science and Technology* **18**, pp. 91-104.

Longwell, J. P., Frost, E. E., and Weiss, M. A. (1953), *Industrial and Engineering Chemistry* **47**, No. 8, pp. 1634-1643.

Mansour, M. S., Bilger, R. W., and Dibble, R. W. (1988), *Twenty-Second Symposium (International) on Combustion*, The Combustion Institute, Pittsburgh, pp. 711-719.

Mansour, M. S., Bilger, R. W., and Stårner, S. H. (1989), *Combustion Science and Technology* **65**, pp. 83-101.

Mansour, M. S., Bilger, R. W., and Dibble, R. W. (1990), "Turbulent Premixed Flames of Methane near Extinction in a Reverse Flow reactor," *Second International Workshop on Turbulent Premixed Combustion*, CNRS, Paris.

Mansour, M. S., Bilger, R. W., and Dibble, R. W. (1991), *Combustion and Flame* **85**, p. 215.

Masri, A. R., Bilger, R. W., and Dibble, R. W. (1987a), *Combustion and Flame* **68**, pp. 109-119.

Masri, A. R., Bilger, R. W., and Dibble, R. W. (1987b), *Combustion and Flame* **71**, pp. 245-266.

Masri, A. R., Bilger, R. W., and Dibble, R. W. (1987c), *Combustion and Flame* **73**, pp. 261-285.

Mellor, A. M. (1994), "NO_x and CO Emissions Models for Gas-Fired, Lean, Premixed Combustion Turbines: AGTSR Semi-Annual Report 1," *Vanderbilt University.*

Nguyen, Q. V., Edgar, B. L., Dibble, R. W., and Gulati, A. (1995), *Combustion and Flame* **100**, pp. 395-406.

Pan, J. C., Vangsness, M. D., Heneghan, S. P., Schmoll, W. J., and Ballal, D. R. (1991a), "Laser diagnostic studies of confined turbulent premixed flames stabilized by conical bluff bodies: Data set", *University of Dayton Report*, UDR-TR-91-102, July.

Pan, J. C., Vangsness, M. D., Heneghan, S. P., and Ballal, D. R. (1991b), "Scalar measurements in bluff body stabilized flames using CARS diagnostics," *ASME Paper No. 91-GT-302.*

Pan, J. C., Schmoll, W. J., and Ballal, D. R. (1992a), Transactions of ASME, *Journal of Engineering for Gas Turbines and Power* **114**, pp. 33-38.

Pan, J. C., and Ballal, D. R. (1992b), "Chemistry and turbulence effects in bluff body stabilized flames," *AIAA Paper No. 92-0771.*

Pope, S. B. (1990), *Twenty-Third Symposium (International) on Combustion*, The Combustion Institute, Pittsburgh, p. 591.

Pratt, D. T. (1980), "Coalescence/Dispersion Modelling of Gas Turbine Combustors," *Gas-Turbine Combustor Problems*, Edt., A. H. Lefebvre, Hemisphere Publishing, New York, NY, pp. 315-334.

Reynolds, W. C. (1986), "The Element Potential Method for Chemical Equilibrium Analysis: Implementation in the Interactive Program STANJAN," *Stanford University.*

Reisel, J. R., Carter, C. D., Laurendeau, N. M. (1993), *Combustion Science and Technology* **91**, pp. 271-295.

Stårner, S. H., Bilger, R. W., Dibble, R. W., and Barlow, R. S. (1990), *Combustion Science and Technology* **21**, pp. 259-276.

Swithenbank, J., Turan, A., and Felton, P. G. (1980), "Three-Dimensional, Two-Phase Modelling Problems of Gas-Turbine Combustors," *Gas-Turbine Combustor Problems*, Edt., A. H. Lefebvre, Hemisphere Publishing, New York, NY, pp. 249-314.

Vranos, A., Knight, B. A., Procia, W. M., and Chiapetta, L. (1992), *Twenty-Fourth Symposium (International) on Combustion*, The Combustion Institute, Pittsburgh, pp. 377-384.